© 2017. Published by The Company of Biologists Ltd | Journal of Cell Science (2017) 130, 3496-3506 doi:10.1242/jcs.202879

RESEARCH ARTICLE

C-terminal motifs in promyelocytic leukemia protein isoforms critically regulate PML nuclear body formation

Chuang Li, Qiongfang Peng, Xiao Wan, Haili Sun and Jun Tang*

ABSTRACT

Promyelocytic leukemia protein (PML) nuclear bodies (NBs), which are sub-nuclear protein structures, are involved in a variety of important cellular functions. PML-NBs are assembled by PML isoforms, and contact between small ubiquitin-like modifiers (SUMOs) with the SUMO interaction motif (SIM) are critically involved in this process. PML isoforms contain a common N-terminal region and a variable C-terminus. However, the contribution of the C-terminal regions to PML-NB formation remains poorly defined. Here, using high-resolution microscopy, we show that mutation of the SIM distinctively influences the structure of NBs formed by each individual PML isoform, with that of PML-III and PML-V minimally changed, and PML-I and PML-IV dramatically impaired. We further identify several C-terminal elements that are important in regulating NB structure and provide strong evidence to suggest that the 8b element in PML-IV possesses a strong ability to interact with SUMO-1 and SUMO-2, and critically participates in NB formation. Our findings highlight the importance of PML C-termini in NB assembly and function, and provide molecular insight into the PML-NB assembly of each distinctive isoform.

KEY WORDS: SIM, PML isoform, PML, PML IV, PML nuclear bodies

INTRODUCTION

Promyelocytic leukemia protein (PML) nuclear bodies (NBs) are a type of nuclear spherical protein structure that range from 0.1 to 1 µm in diameter (Lallemand-Breitenbach and de The, 2010; Sahin et al., 2014a). They are widely distributed in mammalian cells and play an important role in a variety of cellular processes, such as transcription regulation, senescence, apoptosis, DNA repair and antiviral response (Pearson et al., 2000; Zhong et al., 2000b; Bernardi and Pandolfi, 2007; Everett and Chelbi-Alix, 2007; Giorgi et al., 2010; di Masi et al., 2016). Hundreds of proteins have been found to be associated with PML-NBs, either transiently or permanently, which may mediate the diverse functions of PML-NBs (Negorev and Maul, 2001; Weidtkamp-Peters et al., 2008; Shire et al., 2016). Defects in PML-NBs are closely related to pathogenesis, notably tumorigenesis (Salomoni and Pandolfi, 2002; de Thé et al., 2012).

A typical PML-NB is a hollow sphere presenting as a doughnut shape in electron microscopy images (Lallemand-Breitenbach and de The, 2010). PML is the structural component and organizer of PML-NBs (Lallemand-Breitenbach et al., 2001). It belongs to the tripartite motif family with a characteristic RBCC region that includes a RING domain, two B boxes and a coiled-coil (CC) region (Jensen et al., 2001). Six nuclear isoforms of PML derived from alternative mRNA splicing, termed PML-I to PML-VI, are found to co-exist in NBs (Condemine et al., 2006; Nisole et al., 2013). These isoforms share a common N-terminal region containing an RBCC motif, but they differ in their C-termini (Jensen et al., 2001). PML is SUMOylated, primarily at K65, K160 and K490 in the common region (Kamitani et al., 1998). PML-I to PML-V also contain a SUMO-interacting motif (SIM) N-terminal to the variable regions (Kerscher, 2007). PML-VI is the shortest isoform with just a few unique amino acid residues at its C-terminus, and it lacks the SIM (Brand et al., 2010).

Understanding the molecular events governing PML-NB assembly is fundamental for PML-NB biology. Previous studies using one PML isoform, typically PML-IV or PML-VI, have demonstrated that PML multimerization and SUMOylation are critical in promoting NB assembly (Zhong et al., 2000a; Lallemand-Breitenbach et al., 2001). PML multimerization mediated by its CC region initiates PML nucleation, which drives the formation of primary PML aggregates and promotes sumoylation of PML and its associated proteins in a PML RING-dependent manner (Sahin et al., 2014b). Through multiple SUMO–SIM interactions, SUMOylated PML further recruits partner proteins and induces re-organization of the primary PML aggregates into mature NBs, displayed as hollow spheres (Sahin et al., 2014a). Mutations in PML-IV that abolish PML multimerization and SUMOylation severely impair the normal process of PML-NB assembly (Shen et al., 2006).

The PML SIM is considered to be another critical structural component in PML-NB maturation due to its ability to interact with the SUMO moiety of PML (Cappadocia et al., 2015). However, this view has been challenged by some studies, which have shown that SUMOylation or mutation of the SIM in PML-I or PML-III did not have much impact on NB morphology (Cuchet et al., 2011; Sahin et al., 2014b). The main disputed point is if SUMO–SIM interactions between PML are required for the formation of ordered hollow spheres from aggregates (Shen et al., 2006; Sahin et al., 2014b). As these studies used different isoforms, one possibility is that the mechanisms involved in NB formation for different isoforms may not be the same.

Endogenous PML-NBs are assembled by multiple PML isoforms with distinct C-termini; however, attention has mostly focused on the common region of all isoforms (Sahin et al., 2014a). Increasing evidence indicates that the unique C-terminus of each isoform is also functionally important. For instance, the C-terminal portion of PML-IV is critical in p53 regulation and in recruiting specific proteins, such as telomerase reverse transcriptase and the tumor suppressor ARF (officially known as CDKN2A) (Ivanschitz et al., 2015; Oh et al., 2009; Hsu et al., 2012); PML-V-NBs are relatively immobile, which can be attributed to an α-helix within the C-

State Key Laboratory of Agrobiotechnology and College of Veterinary Medicine, China Agricultural University, Beijing 100193, China.

*Author for correspondence (jtang@cau.edu.cn)

C.L., 0000-0002-0271-1397; Q.P., 0000-0002-1997-1574; X.W., 0000-0001-8787-9174; H.S., 0000-0002-1061-5119; J.T., 0000-0002-4540-1647

Received 21 February 2017; Accepted 10 August 2017

Journal of Cell Science

Journal of Cell Science (2017) 130, 3496-3506 doi:10.1242/jcs.202879

terminus (Geng et al., 2012); NBs of different isoforms respond differently in arsenic-induced degradation (Maroui et al., 2012; Hands et al., 2014). However, whether and how these C-terminal regions participate in PML-NB formation is largely unknown. Because these regions are very close to the SIM (Maroui et al., 2012), they could potentially modulate the function of the SIM, thereby influencing the process of NB formation. One strategy to test this is to systematically examine and compare the effect of SIM mutation on the structures of NBs formed by each PML isoform.

Here, using high-resolution microscopy, we found that mutation of the SIM indeed differentially influenced the structure of NBs formed by each individual PML isoform, and we provide evidence to suggest that these differences are due to distinct structural elements in the C-terminus of each isoform. Our findings highlight the importance of PML C-termini in NB assembly.

RESULTS

The SIM differentially affects NB formation by each individual isoform

To determine if the SIM plays a similar role in the NB formation mediated by each individual isoform, we created a SIM-defective mutant for isoforms I to V by substituting VVVI with AAAS (Shen et al., 2006), which we termed PML SIMm (Fig. 1A). In addition, we fused the SIM sequence at the C-terminus of PML-VI and named the fusion protein PML-VI+SIM (Fig. 1A). Plasmids expressing green fluorescent protein (GFP)-tagged WT or PML-I to PML-VI SIMm/+SIM constructs were individually transfected into a PML-knockout (PML-KO) HeLa cell line (Fig. S1), which was generated using the TALEN gene editing technique (Bedell et al., 2012; Carlson et al., 2012). PML-KO was verified by immunofluorescence, western blot analysis and genomic sequencing (Fig. S1). Moreover, we generated a series of HeLa cell lines stably expressing individual PML-I to PML-VI, and their SIMm/+SIM mutants. The stable cell lines expressing cells PML-II to PML-VI were made in PML-KO HeLa cells, while PML-I stable cells were constructed in PML-WT cells as we failed to obtain stable cells using PML-KO cells (Fig. S2). PML-NBs were examined by fluorescence and super-resolution structured illumination microscopy (SR-SIM). NBs were assessed based on several aspects, including mean number, size, homogeneity and hollowness. For hollowness, we primarily focused on the NBs with sizes of approximately 0.5 µm in diameter.

NBs formed by wild-type PML-I to PML-V closely resembled each other compared with those formed by PML-VI in respect to size and homogeneity in both transient transfected cells and stable cell lines (Figs 1B and 2A). These NBs were relatively homogeneous, with a diameter of approximately 0.5 µm (Fig. 2D). In contrast, PML-VI NBs were heterogeneous, many with a diameter close to or even exceeding 1 µm, and some had a diameter of less than 0.2 µm (Figs 1B and 2A,D). In addition, the NBs formed by PML-I, PML-III, PML-IV and PML-V were hollow, while those formed by PML-II and PML-VI were solid (Figs 1C and 2B). To better evaluate PML-NB hollowness, we defined a method to relatively quantify the hollowness of PML-NBs. We first measured fluorescence intensity at the maximal cross-section of a PML-NB to generate a fluorescence intensity curve (Fig. 1D). A hollowed PML-NB generates two peaks. We then determined the points on the *y*-axis which are half the maximum amplitude of each peak. The degree of hollowness is defined as the ratio between the width of two inner points (d1) and that of two outer points (d2) on the *x*-axis (Fig. 1E).

Compared with the NBs formed by WT proteins, SIM mutations in PML-I to PML-V showed a differential impact on NBs of each isoform in both transiently transfected cells (Fig. 1) and stable cell lines (Fig. 2), with that of PML-IV being the most dramatically affected and showing the greatest reduction in mean number and loss of hollowness with a drastic increase in size (Fig. 1B–F and Fig. 2). SIM mutation also greatly affected the NBs of PML-I but generated minimal changes to those formed by PML-II, PML-III and PML-V, in regard to number, size and hollowness (Fig. 1B–F and Fig. 2). Furthermore, addition of SIM to PML-VI converted the NBs from solid large aggregates to hollow spheres with reduced sizes and increased number and homogeneity (Fig. 1B–F and Fig. 2). Western blot analysis following immunoprecipitation showed that SIM mutations did not affect SUMOylation of PML (Fig. 1G). Collectively, these data indicate that PML SIM plays a role in regulating size, number and hollowness of NBs; however, its contribution varies between the different isoforms.

SIM promotes the transformation of PML-VI-NBs by interacting with the SUMO moiety on the K160 site

Addition of the SIM to PML-VI induced a transformation of NBs from solid large aggregates to ordered hollow spheres, shown as ring shapes under SR-SIM, and increased the number of NBs formed (Figs 1B–F and 2). As the PML SIM sequence contains four serine residues, some of which might be phosphorylated, probably by CK2 (Scaglioni et al., 2006), we substituted these four serine residues with four alanine residues (Fig. 3A upper row). Mutating VVVI to AAAS completely abolished the ability of SIM to affect NBs, whereas the S to A mutation only had a partial effect (Fig. 3B–F). Western blot analysis indicated that the SUMOylation levels among all these mutants were comparable (Fig. 3G). In addition, fusing SIM sequences from other proteins, including Daxx (Lin et al., 2006), HIPK2 (Sung et al., 2011), RNF4 (Tatham et al., 2008) and RanBP2 (Song et al., 2004), to PML-VI all induced hollowness in NBs, although the sizes of the formed NBs varied (Fig. 3H). Taken together, these data suggest that the SUMO–SIM interaction, not phosphorylation, is critical in facilitating PML to form more ordered NB structures.

To determine which lysine residue is critical for mediating interactions with the SIM, we mutated K65, K160 and K490, either individually, two in combination or three together, to arginine in PML-VI WT and PML-VI+SIM. The mutant with all three lysines changed to arginine was named 3KR (Fig. 3A, middle row). SR-SIM images showed that the hollowness of the NBs formed by PML-VI+SIM was diminished in NBs formed by the mutants containing a K160R mutation, suggesting that SUMOylation at K160 is critical for NB formation (Fig. 3I). Careful examination of these NBs in comparison with their counterparts without a SIM revealed that the small inner center of these NBs, including that of PML-VI-3KR+SIM, appeared to be hollow (Fig. 3I,J). We therefore suspected that some weak SUMO–SIM interactions may still occur. To further disable SUMOylation, we created a 6KR mutant, in which six SUMOylation sites, including three minor ones (Liang et al., 2016), were mutated (Fig. 3A, lower row). As expected, the NBs formed by PML-VI+SIM-6KR completely lost their hollowness (Fig. 3I,J).

The C-terminal α-helix in PML-V conceals the contribution of the SIM to NB formation

To determine if the resistance of the PML-V-NBs against SIM mutation that we observed above was due to the possibility that the SIM mutant we created may still retain some SUMO binding

Journal of Cell Science (2017) 130, 3496-3506 doi:10.1242/jcs.202879

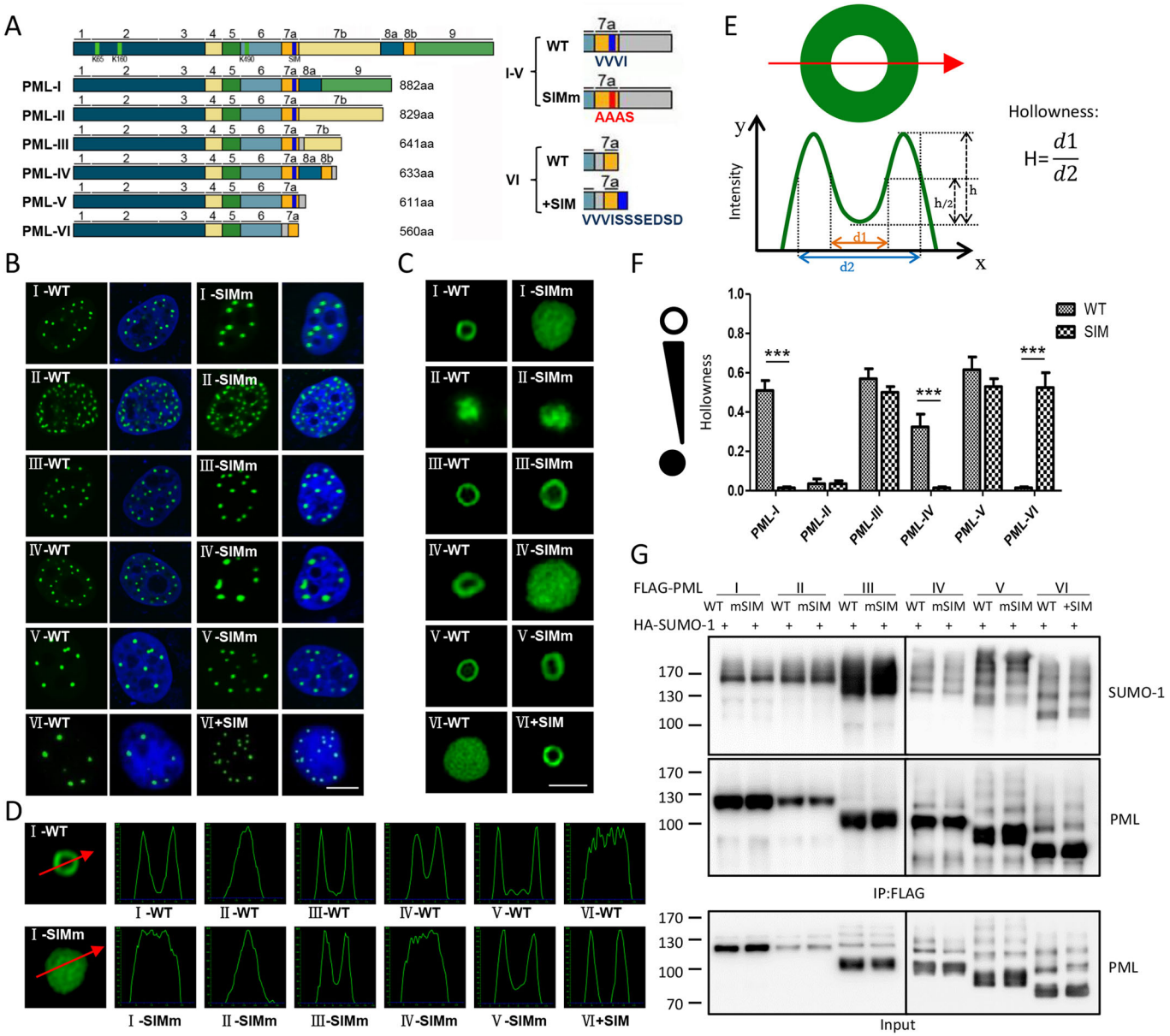

Fig. 1. The SIM differentially affects NB formation by each individual isoform. (A) Schematic representation of PML isoforms I to VI and their SIM mutants. For PML-I to PML-V, SIM mutants refer to the fact that the SIM was mutated; for PML-VI, it means that the SIM was added to the C-terminus of PML-VI. (B) Green fluorescent protein (GFP) fluorescence analysis of PML-NBs formed by PML isoforms and their SIM mutants. PML-KO HeLa cells transfected with plasmids expressing PML mutants as indicated were fixed after 24 h and analysed by GFP fluorescence. Cell nuclei were stained with DAPI. Scale bar: 5 µm. (C) Super-resolution images of NBs of PML isoforms and their SIM mutants. Endogenous expression of single PML-NBs in B was analysed using structured illumination to gain high-resolution images of NBs, and representative images are shown. Scale bar: 1 µm. (D) GFP fluorescence intensity curves of representative NBs of PML isoforms and mutants at the cross-section axis shown by red arrows. (E) A schematic depiction of the method for quantification of the hollowness of a PML-NB. A representation of a hollowed PML-NB and its GFP fluorescence intensity curve are shown. The points on the *x*-axis that are half the maximum height of each peak were determined. The degree of hollowness is defined as the ratio between the width of two inner points (d1) and that of two outer points (d2) on the *x*-axis. (F) The hollowness of NBs of PML isoforms and mutants. For NBs of a specific PML protein, their hollowness is the average number from 12 random chosen PML-NBs in six cells. (G) Comparative analysis of SUMO-1 modification between WT and SIM mutant of each isoform. Cells were co-transfected with HA-SUMO-1 and FLAG-PML isoforms or their SIM mutants. Cell lysates were immunoprecipitated followed by western blot analysis using HA antibodies for SUMO-1 and FLAG antibodies for PML isoforms. Bars and error bars in F represent means and s.d. (*n*=3). ***P<0.001.

activity, we further mutated the SIM region in PML-V (Fig. 4A). SSSEDSD in the SIM was mutated to AAAEDAD, as this sequence has also been reported to be involved in SUMO interaction (Cappadocia et al., 2015), and the mutant was referred to as SIM-SA (Fig. 3A). We also constructed a SIM-VSA mutant in which the SIM sequence of VVVISSSEDSD was changed to AAASAAAEDAD ensuring that the SIM completely lost its SUMO binding ability (Cappadocia et al., 2015) (Fig. 4A). Compared with those of WT and the above SIMm of PML-V, the NBs formed by PML-V-SIM-SA and PML-V-VSA did not change appreciably in number and morphology but became heterogeneous in size (Fig. 4B–E). These results indicated that PML-V indeed had an ability to maintain the ring-shaped structure independently of the SIM. We previously identified a unique α-helix in the C-terminus of

Journal of Cell Science (2017) 130, 3496-3506 doi:10.1242/jcs.202879

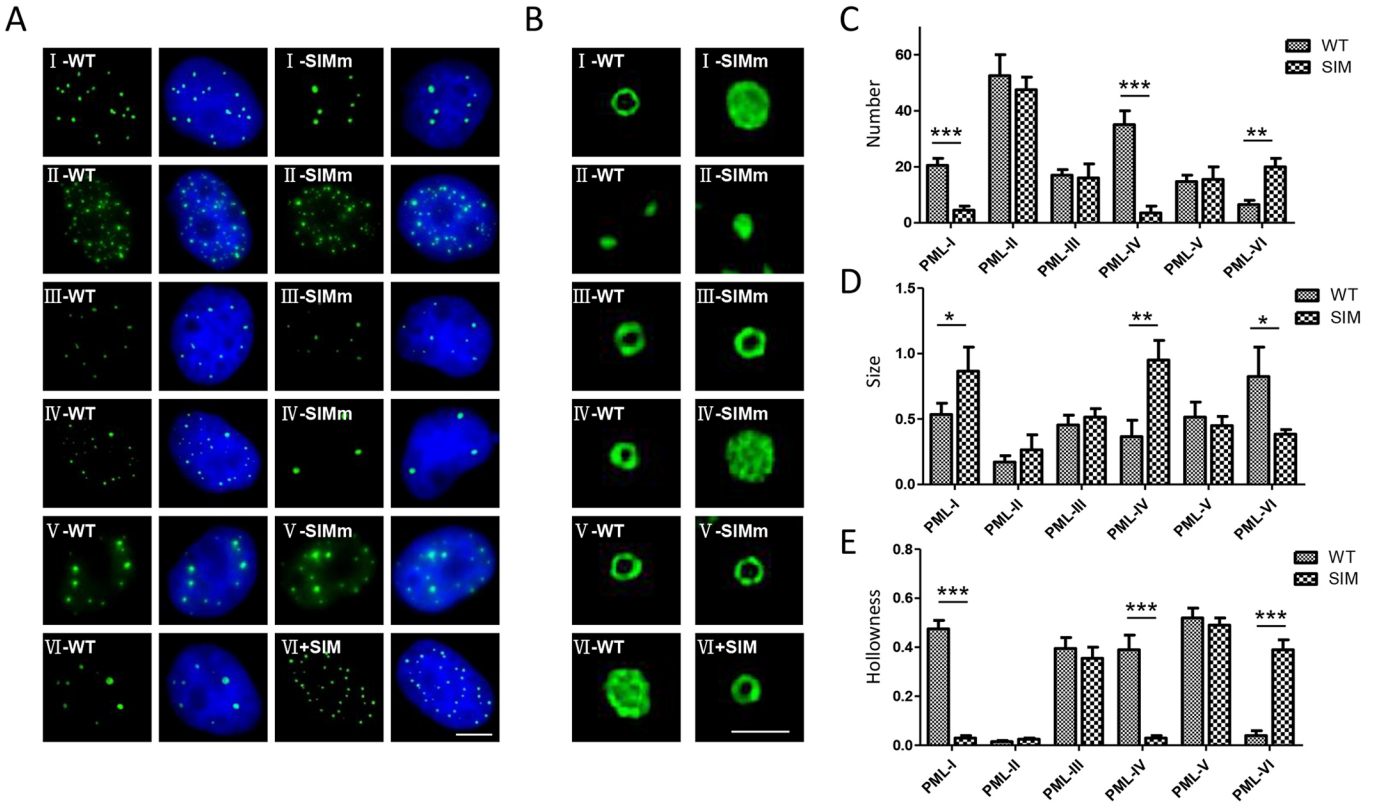

Fig. 2. The SIM differentially affects NB formation in stable cell lines. (A) GFP fluorescence analysis of PML-NBs in HeLa cells stably expressing GFP-tagged PML isoforms and their SIM mutants as indicated. These PML stable cells were stained with DAPI after fixation. Scale bar: 5 µm. (B) Super-resolution structured illumination images of representative NBs from GFP-PML stable cell lines. Scale bar: 1 µm. (C) The average number of PML-NBs per cell from 100 cells was calculated and is shown. (D) Average length of the maximum cross-section of 30 NBs is shown. (E) Hollowness of NBs in each stable cell line. The hollowness of 12 random chosen PML-NBs in six cells was calculated and averaged. Bars and error bars in C, D and E represent mean with s.d. (n=3). *P<0.05; **P<0.01; ***P<0.001.

PML-V capable of mediating strong protein–protein interactions and immobilizing PML-V-NBs (Geng et al., 2012). Strikingly, mutation of the SIM in this α-helix-defective mutant (PML-V-RP) generated a huge impact on the NBs formed, similar to the effect on NBs formed by PML-I/PML-IV with a SIM mutation, in comparison with that of the SIM WT counterpart (Fig. 4B,C). These changes included a decrease in the number of NBs, a size increase and abolition of the ring-shaped structure (Fig. 4D–F). Collectively, these data suggest that in the presence of the C-terminal α-helix, the role of the SIM in NB formation is masked.

The role of the SIM in PML-IV-NB formation is related to its 8b region

Mutation of the SIM in PML-IV produced the most dramatic impact on the formation of NBs (Figs 1 and 2). To explore whether this effect is related to its 8a or 8b region, we deleted these two regions from PML-IV (Fig. 5A). Strikingly, the NBs formed by the 8b deletion mutant (PML-IV-Δ8b), regardless of the SIM mutation, were significantly enlarged and lost hollowness, a phenotype that resembled that of the SIM-defective mutant of PML-IV (Fig. 5B,C). Compared with WT, the number of NBs was reduced and was further decreased by SIM mutation (Fig. 5D). In contrast, 8a deletion did not yield any apparent alterations in the morphology and size of NBs, but the effect of further SIM mutation was dramatic (Fig. 5B,C). The differential effect of 8b and 8a deletion on PML-IV-NBs was verified in PML-KO HeLa cells that stably expressed GFP-PML-IV-Δ8b or GFP-PML-IV-Δ8a mutant (Fig. S3). Western blot analysis indicated that the SUMOylation levels among all these mutants were comparable (Fig. 5F). Failure of PML-IV-Δ8b to form the expected hollow NB structures suggests an intriguing possibility that the structural role of the SIM in this mutant is suppressed by 8a. To test this, we fused 8a to PML-IV+SIM and observed the disruption of the hollow structure of NBs as predicted (Fig. 5G,H). Taken together, these data indicate that 8b is critically involved in PML-IV-NB formation and is functionally related to SIM, whereas 8a has an ability to interfere with SIM function.

8b of PML-IV possesses the ability to bind with SUMO

To explore the role of 8b in the formation of NBs, we fused 8b to the C-terminus of PML-VI (Fig. 6A upper row) and generated GFP-PML-VI+8b stable cell lines. Addition of 8b to PML-VI increased the number and homogeneity of NBs (Fig. 6B,D). In addition, the size of the NBs was decreased and hollowness was induced (Fig. 6C,E). All of these changes in NBs were remarkably similar to those caused by adding a SIM to PML-VI, suggesting the possibility that 8b may function as a SIM. To test this, we examined the interaction between 8b and SUMO-1/SUMO-2 using a yeast two-hybrid assay, in which the Daxx C-terminal SIM was replaced with 8b or PML-SIM (Fig. 6F,G). The results showed that 8b displayed a strong SUMO-1 and SUMO-2 binding ability, particularly to SUMO-1, which was even stronger than that of PML-SIM (Fig. 6G). In addition, we examined the direct interaction between 8b and SUMO-1/SUMO-2 using *in vitro* glutathione S-transferase (GST) pull-down assays. The results show that 8b directly binds

Journal of Cell Science (2017) 130, 3496-3506 doi:10.1242/jcs.202879

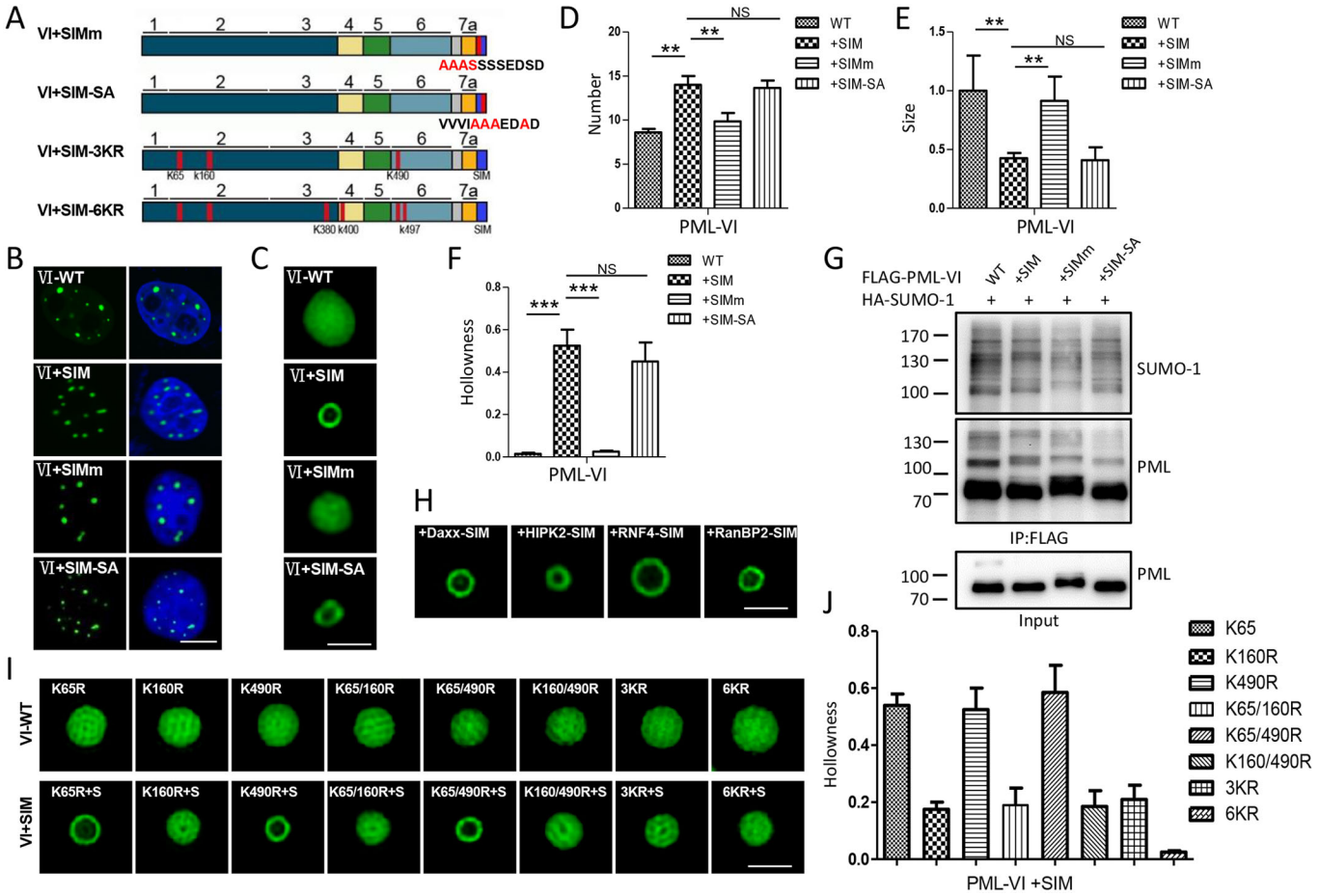

Fig. 3. SIM promotes the transformation of PML-VI-NBs by interacting with the SUMO moiety on K160. (A) Schematic representation of PML-VI+SIM mutants with the hydrophobic region, serine-rich region or SUMOylation sites mutated. Three major SUMOylation sites (K65/K160/K490) were replaced by arginine (3KR), and 6KR includes three new-found additional SUMOylation sites (K380/K400/K497). (B) GFP fluorescence analysis of PML-NBs formed by PML-VI+SIM mutants. PML-KO HeLa cells transfected with GFP-PML-VI+SIM mutants were fixed and analysed by GFP fluorescence; nuclei were stained with DAPI. Scale bar: 5 µm. (C) Super-resolution images of NBs of PML-VI+SIM mutants. Single PML NB was analysed using structured illumination, and representative images are shown. Scale bar: 1 µm. (D) The average number of PML NBs per cell from 100 cells was calculated and is shown. (E) The average length of the maximum cross-section of 30 NBs is given. (F) The average hollowness of 12 PML-NBs is shown. (G) Influence of SIM mutation on PML-VI SUMO-1 modification level. FLAG-tagged PML-VI+SIM mutants were co-expressed with HA-SUMO-1. Lysates were analysed by western blot following immunoprecipitation. (H) Super-resolution structured illumination analysis showing that the SIMs of PML-NB partner proteins can also transform PML-VI NBs. The SIMs of Daxx/HIPK2/RNF4/RanBP2 were added to the C-terminus of PML-VI. Scale bar: 1 µm. (I) Super-resolution images of representative NBs of PML-VI/+SIM and their SUMOylation site mutants. PML-VI/+SIM with single, double or tripartite SUMOylation sites (K65/K160/K490) mutated were transfected into PML-KO HeLa cells. The cells were fixed 24 h post transfection and analyzed using structured illumination. Scale bar: 1 µm. (J) The average hollowness of 12 NBs of GFP-PML-VI +SIM and their SUMOylation site mutants was calculated and is shown. Bars and error bars in D, E, F and J represent mean with s.d. (n=3). $^{**}P$<0.01; $^{***}P$<0.001; NS, not significant.

SUMO-1 or SUMO-2, and that the interaction between 8b and SUMO-1 is stronger than that of SIM and SUMO-1 (Fig. 6H). Collectively, these data suggest that 8b contributes to NB formation by functioning as a SIM.

The ability of PML-IV 8b to regulate p53 depends on the SIM

Mutation of the SIM in PML-IV abolished the normal ring-shaped structure of NBs, indicating that the ability of 8b to promote NB formation was also affected by the SIM mutation (Fig. 5C). PML-IV is critically involved in p53 SUMOylation and cellular senescence (Pearson and Pelicci, 2001; Peche et al., 2012). A recent study indicated that 8b was crucial for this activity of PML-IV. Indeed, co-expression of PML-IV with p53 enhanced p53 SUMOylation, while the 8b deletion mutant failed to do so (Ivanschitz et al., 2015). We then examined whether the ability of 8b to regulate p53 SUMOylation was also regulated by the SIM. As expected, mutation of the SIM diminished the ability of PML-IV to stimulate p53 SUMOylation, indicating that the SIM is required for the function of 8b (Fig. 7).

DISCUSSION

Our results suggest that the ability of the SIM to promote the re-organization of PML-NBs by interacting with SUMO is differentially influenced by the distinct C-terminal region of each isoform. The current model primarily emphasizes the role of the common region of all PML isoforms in PML-NB formation (Sahin et al., 2014a). We extended this model by showing that the C-terminal region of each isoform also critically participates in the process of PML-NB formation. In particular, we found that the contribution of PML-V-SIM to PML-V-NB formation was overshadowed by its C-terminal α-helix, and the 8b region in PML-IV strongly promoted NB formation and was regulated by the

Journal of Cell Science

Journal of Cell Science (2017) 130, 3496-3506 doi:10.1242/jcs.202879

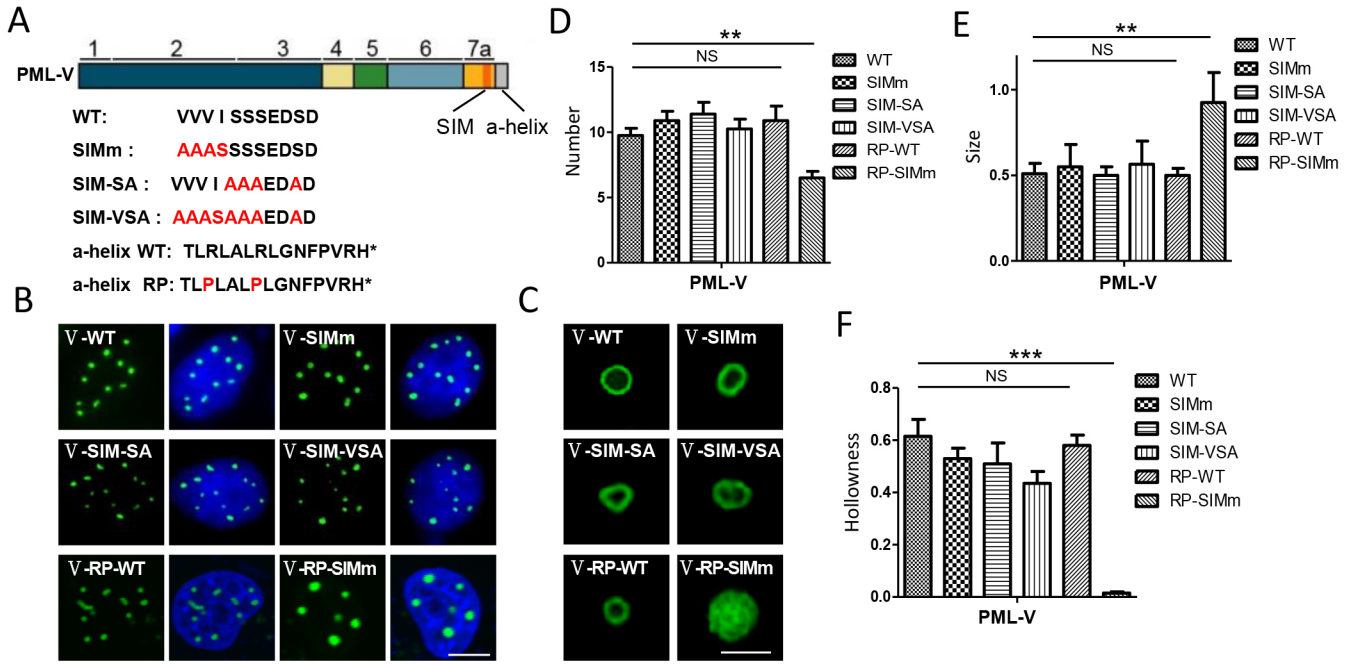

Fig. 4. The C-terminal α-helix in PML-V conceals the contribution of SIM to NB formation. (A) Schematic diagram of the SIM mutants and α-helix mutants of GFP-PML-V. The α-helix in the PML-V C-terminus is destroyed by mutating two arginine residues to prolines, with or without additional mutation of the SIM. (B) Fluorescence analysis of the role of the α-helix in stabilizing PML-V-NBs resistant to SIM mutation. PML-KO HeLa cells were transfected with plasmids expressing GFP-PML-V or its α-helix mutants. Cells were fixed after 24 h and analysed by GFP fluorescence. Cell nuclei were stained with DAPI. Scale bar: 5 µm. (C) Super-resolution images of representative NBs of PML-V and its mutants. Endogenous expression of single PML-NB in B was analysed using structured illumination to gain high-resolution images of NBs, and representative images are shown. Scale bar: 1 µm. (D) Quantification of PML-NBs of PML-V and its mutants. The average number of PML-NBs per cell from 100 cells was calculated and is shown. (E) Average length of the maximum cross-section of 30 NBs is shown. (F) Average ratio of hollowness of 12 random NBs from six PML-KO cells transfected with GFP-PML mutants was calculated and is shown. Bars and error bars in D, E and F represent mean with s.d. (n=3). $^{**}P$<0.01; $^{***}P$<0.001; NS, not significant.

SIM (Fig. 4). Our studies highlight the importance of PML C-termini in NB formation and their interplay with SIMs.

For simplicity, we can divide the process of PML-NB formation into three phases: the first phase refers to PML multimerization driven by the N-terminal RBCC region to form solid protein aggregates of various sizes; in the second phase, the PML aggregates reorganize and assemble into ordered hollow spheres, displayed as ring-shapes under high-resolution microscopy; and in the third phase, other proteins are recruited into the PML-NBs (Ishov et al., 1999; Lallemand-Breitenbach et al., 2001; Lallemand-Breitenbach and de The, 2010; Lang et al., 2010). Although the three phases are coherent, inseparable and all important for the normal structure and function of PML-NBs, we primarily focus on the second phase, particularly on understanding the mechanism that induces reorganization with respect to distinct isoforms.

A disputed point in the mechanism of PML-NB formation is whether SUMO–SIM interactions are required for a PML-NB to progress from phase I to phase II (Shen et al., 2006; Sahin et al., 2014b). Studies with PML-IV indicate that the SUMO–SIM interactions are required (Shen et al., 2006), while work with PML-III showed otherwise (Cuchet et al., 2011; Sahin et al., 2014b). Indeed, in our study, SIM mutation in PML-IV blocked the PML-NB transformation, whereas that of PML-III had little effect (Fig. 1). Our results suggest that this inconsistency stems from the unique C-terminal region of each isoform. Without the influence of the C-terminal tail, as in the case of PML-VI when a SIM was added, SUMO–SIM interactions play a major role in inducing PML-NB transformation (Fig. 3).

For other isoforms, the contribution of the SUMO–SIM interaction is differentially modulated by the C-terminal sequences. PML-V contains one α-helix in its C-terminus. This motif possesses a strong ability to mediate protein–protein interactions, which may facilitate and stabilize the ordered structure of NBs (Weidtkamp-Peters et al., 2008; Brand et al., 2010; Geng et al., 2012). In the presence of this α-helix, the role of SIM is masked. Only when this stabilizing force is disrupted is the effect of the SUMO–SIM interaction manifested (Fig. 4). Most likely, due to these dual effects, the PML shell in PML-V-NBs is much thinner and more compact than that of the other NBs (Fig. 1C). Although we did not explore whether the C-terminal portion of PML-III was involved in PML-NB formation, we predict it would be the case and, like PML-V, both the SIM and C-terminal tail of PML-III may positively and independently induce PML-NB transformation. For PML-I and PML-IV, SIM mutations reversed PML-NB formation from phase II to phase I, indicating that the SIM is required and necessary for their NB formation (Fig. 1C). PML-II did not form the typical ring-shaped structures observed with the other isoforms with a SIM (Brand et al., 2010; Ohsaki et al., 2016). This could be due to the cell type that we used or to the fact that PML-II has a long C-terminal portion that interferes with SUMO–SIM interactions required for the ring-shaped NB formation (Brand et al., 2010).

The role of the SIM in PML-IV is probably not limited to mediating interactions with SUMO, but more importantly, it regulates the functions of the 8b region. PML-IV is the only isoform that can activate p53 and induce cellular senescence upon over-expression, and thus it has been extensively studied (Peche et al., 2012; Ivanschitz et al., 2015; Fukuda et al., 2017). A recent study reported that the 8b region could interact with ARF and promote global SUMOylation, particularly that of p53 (Ivanschitz et al., 2015). This region is also involved in specific interactions

Journal of Cell Science (2017) 130, 3496-3506 doi:10.1242/jcs.202879

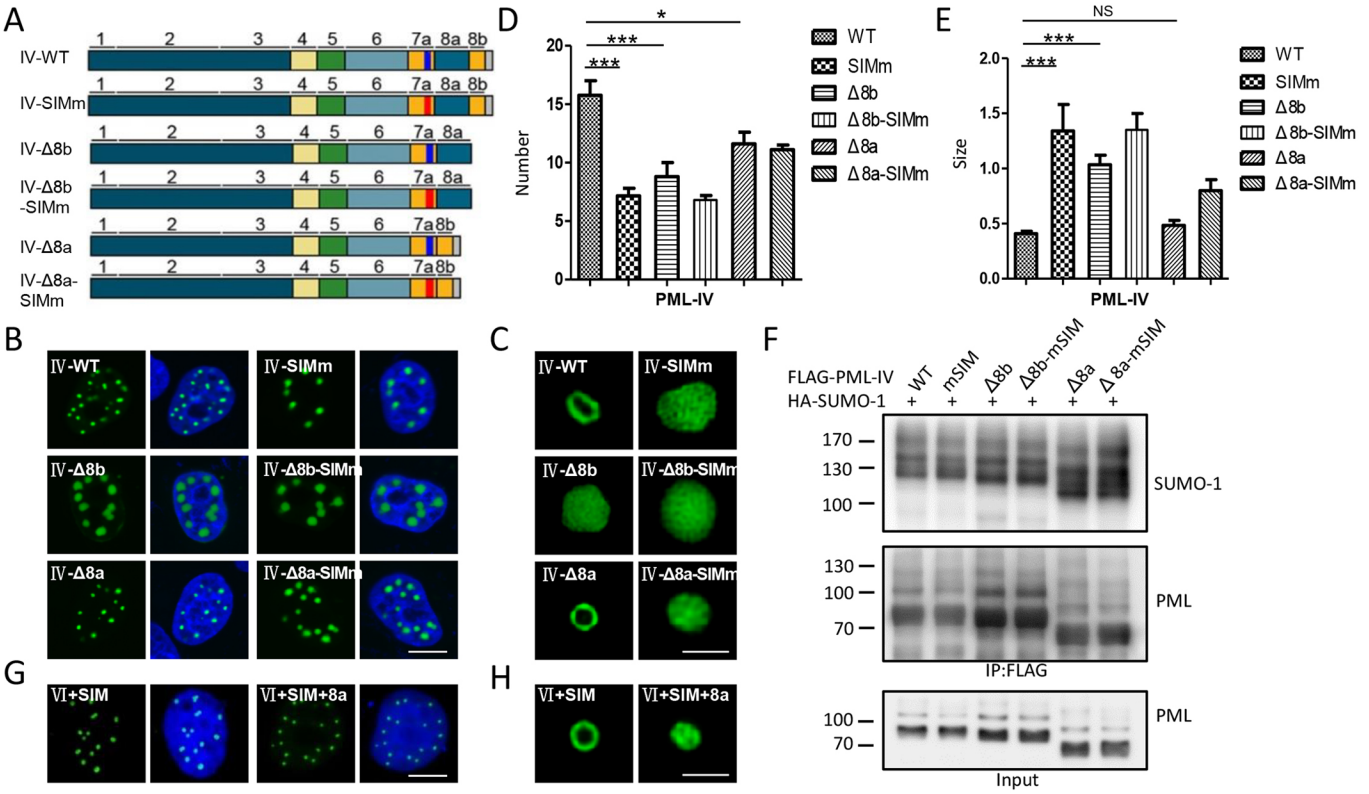

Fig. 5. The role of the SIM in PML-IV-NB formation is related to its 8b region. (A) Schematic diagram of the deletion and point mutants of GFP-PML-IV. Exon 8a or 8b in the PML-IV C-terminus is deleted, with SIM additionally mutated. (B) Fluorescence images of PML-NBs formed by the PML-IV mutants. PML-KO HeLa cells were transfected with plasmids expressing GFP-PML-IV or its mutants. Cells were fixed after 24 h and analysed by GFP fluorescence. Cell nuclei were stained with DAPI. Scale bar: 5 µm. (C) Super-resolution structured illumination images of representative NBs formed by the PML-IV mutants in B. Scale bar: 1 µm. (D) The average number of PML-NBs calculated from 100 cells for each transfection in B was calculated and is shown. (E) The average length of the maximum cross-section of 30 NBs is shown. (G) Comparison of SUMOylation levels of PML-IV and its mutants. Flag-PML-IV or its mutants and HA-SUMO-1 were over-expressed in PML-KO HeLa cells for 24 h, purified over M2 beads and subjected to western blot analysis using anti-FLAG and anti-HA antibodies. (G) Fluorescence analysis of the effect of 8a on the formation of PML-VI+SIM NBs. PML-KO HeLa cells were transfected with GFP-PML-VI+SIM/+SIM+8a, and images were taken 24 h after transfection. Scale bar: 5 µm. (H) Super-resolution images of NBs formed by PML-VI+SIM/+SIM+8a. Representative PML-NB images are shown. Scale bar: 1 µm. Bars and error bars in D, E and F represent mean with s.d. (n=3). *P<0.05; ***P<0.001; NS, not significant.

with other proteins, such as certain viral proteins (Maroui et al., 2011; Reichelt et al., 2011; El Asmi et al., 2014) and the pathogenic poly Q protein Htt (Guo et al., 2014). We revealed that 8b also played a critical role in PML-NB formation because deletion of 8b disrupted the ring-shaped structure despite the presence of the SIM, whereas adding 8b to the C-terminus of PML-VI induced these structures (Figs 5C and 6). The function of the SIM is probably suppressed by 8a in PML-IV as both PML-IV-Δ8b and PML-VI +SIM+8a failed to form the ring-shaped structure (Fig. 5C,I). The ability of 8b to promote PML-NB formation depends on the functionality of SIM, as the ring-shaped structures of PML-IV-NBs were disrupted upon SIM mutation (Fig. 5C). Consistently, the ability of 8b to enhance p53 SUMOylation was also lost (Fig. 7). It seems that the SIM, 8a and 8b form a complex relationship. It is possible that 8a could be a negative module for both the SIM and 8b. When the SIM is functional, 8a may lean towards the SIM and block its activity, allowing 8b to exert its function. However, when the SIM loses its functionality, 8a may shift to 8b and suppress its function, resulting in disappearance of the ring-shaped structure. More studies are needed to clarify the relationship between these three motifs.

An interesting finding is that 8b possesses the ability to interact with SUMO. Yeast two-hybrid analysis indicated that 8b could bind both SUMO-1 and SUMO-2, and its interaction with SUMO-1 is even stronger than that of PML-SIM (Fig. 6G). The three conserved bulky hydrophobic AAs, which are critical for regulating p53 (Ivanschitz et al., 2015), are required for 8b–SUMO-1 interaction (Fig. 6F). Thus, to a certain degree, 8b may function as a SIM, which may explain its ability to regulate the formation of NBs. The discovery that 8b and the SIM share certain properties suggests that 8a could inhibit the SIM and 8b using a similar mechanism. One potential mechanism is that SUMOylation at K616 in 8a may interact with PML-SIM or 8b, thereby inhibiting their function (Sung et al., 2011). Several important functions of PML-IV are attributed to 8b (El Asmi et al., 2014; Ivanschitz et al., 2015). The discovery of 8b binding to SUMO may help to understand the unique functions of PML-IV. It has been recently reported that PML-IV can mediate global hyper-SUMO-1 conjugation (Hands et al., 2014; Sahin et al., 2014b). It would be interesting to determine if this function of PML-IV is related to the strong ability of 8b to bind with SUMO-1.

In conclusion, we suggest that the variable regions of PML isoforms critically regulate the process of NB formation. The SIM in PML not only participates in NB formation and protein recruitment, but also regulates the function of 8b in PML-IV. In addition, 8b has strong SUMO binding activity, which may relate to the unique functions of PML-IV.

Journal of Cell Science (2017) 130, 3496-3506 doi:10.1242/jcs.202879

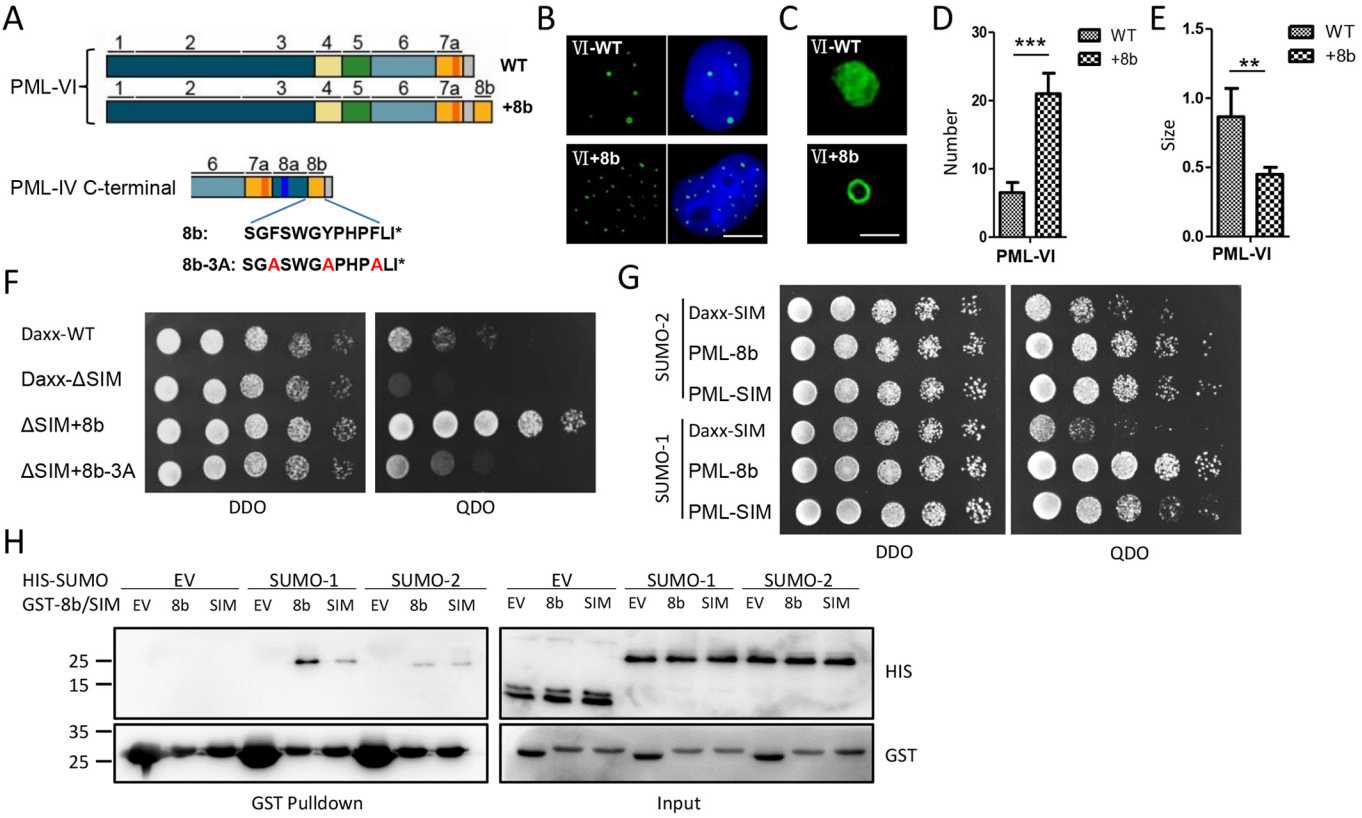

Fig. 6. The 8b of PML-IV possesses the ability to bind with SUMO. (A) Schematic representation of PML-VI with 8b added to its C-terminus. The amino acid sequence of 8b is shown. (B) Fluorescence analysis of NBs formed in GFP-PML-VI-WT/+8b stable cell lines. Scale bar: 5 µm. (C) Super-resolution images of GFP-PML-VI-WT/+8b NBs. Scale bar: 1 µm. (D) Quantification of NBs formed by PML-VI-WT/+8b stable cell lines. The average number of PML-NBs was calculated from 100 cells and is shown. (E) The average length of the maximum cross-section of 30 NBs from stable cell lines is shown. (F) Identification of 8b as a secondary SIM via yeast two-hybrid assay. 8b was added to the C-terminus of Daxx with SIM deletion encoded in a pGBKT7 vector. The constructs were co-transfected with SUMO-1-pACT2 in yeast, and these yeasts were distributed to grow on plates following a serial dilution (1:5). (G) Interaction of 8b with SUMO-1 and SUMO-2 in comparison with the SIMs of Daxx and PML. The SIMs of Daxx and PML and the 8b of PML-IV were respectively added to the C-terminus of Daxx without a SIM in a pGBKT7 vector. The constructs were co-transfected with SUMO-1 or SUMO-2 encoded in a pACT2 vector in yeast cells, and the yeast two-hybrid assay was performed as described. (H) Interaction of PML-8b with SUMO-1 and SUMO-2 *in vitro*. GST or GST-8b/SIM and HIS or HIS-SUMO-1/SUMO-2 were bacterially expressed and mixed with each other as indicated followed by GST beads pull-down and western blotting analysis. Bars and error bars in D and E represent mean with s.d. (n=3). $^{**}P$<0.01; $^{***}P$<0.001.

MATERIALS AND METHODS

Construction of plasmids

Plasmids expressing Flag-PML-I to -IV were previously described (Geng et al., 2012) and used as templates for the following constructions. pBABE-GFP-I to -IV were constructed by subcloning each corresponding PML isoform into the pBABE puro vector between the BamHI and HindIII sites. PML-(I–V)-SIMm and PML-V-RP-SIMm mutants were generated by replacing the amino acids VVVI with AAAS at positions 556–559. The PML-V-RP mutant was described previously (Geng et al., 2012). PML-VI +SIM was created by fusing the SIM sequence of PML (VVVISSSEDSD) to the PML-VI C-terminus. An array of PML-VI KR mutants of WT and +SIM were generated by mutating the lysine residue at positions K65, K160 and K490 to arginine, either individually, two in combination or three together (3KR), and with three additional SUMOylation sites mutated (K380/K400/K497) (6KR) using PCR. PML-IV deletion mutants were generated by PCR. All of the above mutants were either subcloned into the FLAG-pRK5 or the GFP-pBABE puro vector or both. The plasmids used for generating stable cell lines were constructed by inserting GFP-PML-I to -VI and their mutants into the pBABE hygro vector.

For the yeast two-hybrid assay, the C-terminal fragment of Daxx (570–780) (Daxx-C-WT), its C-terminal SIM deletion mutant (Daxx-C-ΔSIM) and Daxx-C-SIM mutants in which the Daxx-C-SIM was replaced with the 8b region of PML-IV (PML-IV-8b) or the SIM of PML (PML-SIM) were cloned into the yeast expressing vector pGBKT7 (Clontech). SUMO-1/SUMO-2 was cloned into another yeast expressing vector pACT2 vector (Clontech). For the GST pull-down assay, 8b/SIM and SUMO-1/SUMO-2 were cloned into bacterial expression vectors pGEX-1ZT (GST tag) and pET30a (HIS tag), respectively.

Primer sequences are listed in Table S1. All mutants were constructed using standard molecular biology techniques and were confirmed by sequencing.

Cell culture and transfection

Cells were cultured in Dulbecco's modified Eagle's medium (DMEM) (Macgene) supplemented with 10% fetal bovine serum (Gemini), 100 U/ml penicillin and 100 U/ml streptomycin at 37°C in a humidified incubator supplied with 5% CO_2. Transient transfections were performed using Lipofectamine 2000 (Invitrogen), or jetPRIME (Polyplus) following the manufacturer's protocol.

PML knock-out HeLa cells

PML-KO HeLa cells were generated using TALEN technology (Bedell et al., 2012). The target sequences of TALEN were as follows: left arm-CTGAAGGCCGCCAGCCCA- and right arm-AACCCAATAGTACCTC-TGT-. Plasmids were constructed by Sidansai Biotechnology (Shanghai, China). The positive PML-KO clones were selected by puromycin at 12.5 µg/ml and validated using immunofluorescence studies, western blotting and genomic sequencing around the target site.

Journal of Cell Science (2017) 130, 3496-3506 doi:10.1242/jcs.202879

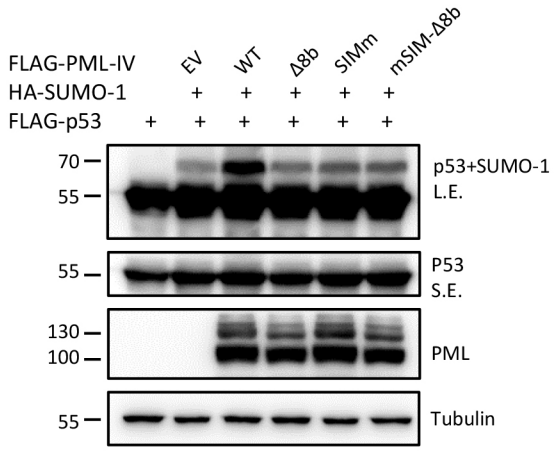

Fig. 7. The ability of PML-IV 8b to regulate p53 depends on the SIM. Western blot analysis of the effect of the SIM on PML-IV 8b-induced increase in the p53 SUMOylation level. PML-KO HeLa cells were transfected with the plasmids expressing the indicated proteins for 24 h and then subjected to western blot analysis. p53 protein was detected by anti-p53 antibody, and SUMOylation of p53 was revealed after longer exposure.

Generation of stable cell lines

pBABE hygro plasmids encoding GFP-PML-(I–VI) WT or mutants were transfected into Phoenix retrovirus packaging cells. Forty-eight hours later, the supernatants containing viral particles were harvested, and then used to infect PML-KO HeLa cells. Cells stably expressing GFP-PML were selected by treating the infected cells with hygromycin at 150 µg/ml for 3 weeks. The PML-I stable cell line was generated in PML-WT HeLa cells following the same procedure except using GFP-PML pBABE puro plasmid for transfection and 12.5 µg/ml of puromycin for selection for 1 week.

Antibodies and chemicals

Anti-HA (Y-11 SC-805), p53 (DO-1, SC-126), anti-SUMO-1 (FL-101 SC-9060) and anti-PML (H-238 SC-5621) antibodies were purchased from Santa Cruz Biotechnology (Santa Cruz, CA, USA). FLAG (M2 F-1804) antibodies, Triton X-100 and *N*-ethylmaleimide (NEM) were purchased from Sigma (St Louis, MO, USA). Anti-α-Tubulin mAb PM054 was purchased from MBL. DAPI (4,6-diamidino-2-phenylindole) was purchased from Beyotime Institute of Biotechnology. Sodium dodecyl sulfate (SDS) was purchased from Scientific Research Ievei. DL-Dithiothreitol (DTT) and bovine serum albumin fraction (BSA) were purchased from Amresco Biotechnology. Puromycin and hygromycin were also purchased from Amresco. Antibodies were diluted at 1:2000 for western blotting and 1:200 for immunofluorescence.

GFP fluorescence

Cell staining was performed as described previously (Geng et al., 2012). In brief, PML-KO HeLa cells grown on glass coverslips in 24-well plates were transfected with up to 0.3 µg of plasmids expressing GFP-PML mutants for 24 h. Cells were then fixed for 30 min with 4% paraformaldehyde (Sinopharm Chemical Reagent Co., Ltd) at room temperature and then stained with 0.1 µg/ml DAPI for 5 min. For calculation and analysis of the average number of PML nuclear bodies in each experiment, more than 100 cells expressing middle to low levels of proteins were observed to avoid artefacts of over-expression.

Microscopy image acquisition

Images of PML-NBs were captured using an Eclipse Ni-E microscope (Nikon Instruments, USA). Data acquisition was performed using a SPOT camera (Diagnostic Instruments, Inc.) and NIS-Elements BR software (Nikon). Images are presented as the maximal intensity projections of a *z*-stack.

Endogenous expression of single PML-NB was observed using a Nikon Eclipse Ti microscope. Images were captured at single *z*-slices to visualize the hollow structure of the PML-NBs by Nikon SR-SIM. Five translations and three rotations of the illumination pattern were obtained and reconstructed with NIS-Elements AR software (Nikon).

Western blotting and immunoprecipitation

The cell lysates were prepared using lysis buffer (50 mM Tris-Cl at pH 8.0, 150 mM NaCl, 1.0% Triton X-100, 10% glycerol, 20 mM NaF, 1 mM DTT, and 1× complete protease mixture). Protein samples were resolved by SDS-PAGE and transferred onto a PVDF membrane (Millipore). The membrane was blocked in 5% skimmed milk in 0.1% Tween-20/PBS and probed with the indicated antibodies followed by incubation with sheep anti-mouse or anti-rabbit IgG-HRP (Santa Cruz Biotechnology). Detection was performed using an ECL detection kit (CW Biotech). To analyse the SUMOylation level of PML mutants, individual FLAG-PML mutants and HA-SUMO-1 were co-expressed in PML-KO HeLa cells. The expression of FLAG-PML mutants was adjusted to similar levels by varying the amount of the plasmids transfected. The cells were lysed in 1% SDS lysis buffer supplemented with 1×complete protease cocktail and 10 mM NEM, followed by 5 min of boiling and sonication (Hands et al., 2014; Sahin et al., 2014b). Immunoprecipitation was then performed with anti-FLAG M2 beads for 4 h at 4°C, after cell extracts were diluted with lysis buffer 10 times. Beads were washed three times in lysis buffer and then eluted with sample buffer. Precipitated complexes were subject to western blotting.

Yeast-directed binding assay

The yeast two-hybrid system we used was described previously (Geng et al., 2012; Zhang et al., 2017). Briefly, the pGBKT7 plasmids expressing the C-terminal fragments of Daxx mutants were co-transformed with pACT2 plasmids expressing SUMO-1 or SUMO-2 into AH109 cells according to standard procedures (Stehmeier and Muller, 2009). For each combination, a group of more than 50 yeast clones were selected. The presence of 'bait' and 'prey' proteins in co-transformed cells was indicated by growth on double drop-out (DDO) plates devoid of leucine and tryptophan in the media. The interactions were scored positive if the co-transformed cells were also able to grow on quadruple drop-out (QDO) plates devoid of leucine, tryptophan, histidine and adenine. To visualize the strength of the interaction, serial dilutions (1:5) with an initial OD of 0.4 were spotted. Empty vector served as a negative control (data not shown).

GST pull-down assay

The direct interaction between 8b and SUMO-1/SUMO-2 was analysed by GST pull-down *in vitro*. The plasmids expressing GST or GST-8b/-SIM and HIS or HIS-SUMO-1/SUMO-2 were transformed into bacterial strain BL21 (DE3) separately. Recombinant protein expression was induced by IPTG for 8 h at 4°C. The bacterial cells were lysed by sonication, and the cell lysates were centrifuged at 13,800 ***g*** for 15 min. The supernatants containing GST or GST fusion proteins were mixed with that of HIS or HIS-tagged proteins, and then co-incubated with GST beads for 3 h at 4°C. After washes, GST beads bound with proteins were analysed by SDS-PAGE followed by western blotting with anti-GST and anti-HIS antibodies.

Statistical analysis

GraphPad Prism (LaJolla, CA, USA) was used for statistical analyses. Error bars represent means±s.d. (n=3). Statistical significance was analysed by Student's *t*-test and expressed as a *P*-value. *P*-values of <0.05 were considered to be statistically significant: $*P<0.05$; $**P<0.01$; $***P<0.001$.

Acknowledgements

We thank Dr Xiaolu Yang at the University of Pennsylvania for the SUMO-1 and SUMO-2 plasmids, and Dr Huiqiang Lou at China Agricultural University for helping with the yeast two-hybrid assay.

Competing interests

The authors declare no competing or financial interests.

Author contributions

Conceptualization: C.L., Q.P., X.W., H.S., J.T.; Methodology: C.L., Q.P., X.W., J.T.; Software: C.L.; Validation: J.T.; Formal analysis: C.L., J.T.; Investigation: C.L., Q.P., X.W., H.S., J.T.; Resources: X.W., H.S., J.T.; Data curation: C.L.; Writing - original draft: C.L., J.T.; Writing - review & editing: C.L., J.T.; Visualization: C.L., J.T.; Supervision: J.T.; Project administration: J.T.; Funding acquisition: J.T.

Funding
This work was supported by the National Natural Science Foundation of China (31371351).

Supplementary information
Supplementary information available online at
http://jcs.biologists.org/lookup/doi/10.1242/jcs.202879.supplemental

References

Bedell, V. M., Wang, Y., Campbell, J. M., Poshusta, T. L., Starker, C. G., Krug, R. G., II, Tan, W., Penheiter, S. G., Ma, A. C., Leung, A. Y. H. et al. (2012). *In vivo* genome editing using a high-efficiency TALEN system. *Nature* **491**, 114-118.
Bernardi, R. and Pandolfi, P. P. (2007). Structure, dynamics and functions of promyelocytic leukaemia nuclear bodies. *Nat. Rev. Mol. Cell Biol.* **8**, 1006-1016.
Brand, P., Lenser, T. and Hemmerich, P. (2010). Assembly dynamics of PML nuclear bodies in living cells. *PMC Biophys.* **3**, 3.
Cappadocia, L., Mascle, X. H., Bourdeau, V., Tremblay-Belzile, S., Chaker-Margot, M., Lussier-Price, M., Wada, J., Sakaguchi, K., Aubry, M., Ferbeyre, G. et al. (2015). Structural and functional characterization of the phosphorylation-dependent interaction between PML and SUMO1. *Structure* **23**, 126-138.
Carlson, D. F., Tan, W., Lillico, S. G., Stverakova, D., Proudfoot, C., Christian, M., Voytas, D. F., Long, C. R., Whitelaw, C. B. A. and Fahrenkrug, S. C. (2012). Efficient TALEN-mediated gene knockout in livestock. *Proc. Natl. Acad. Sci. USA* **109**, 17382-17387.
Condemine, W., Takahashi, Y., Zhu, J., Puvion-Dutilleul, F., Guegan, S., Janin, A. and de Thé, H. (2006). Characterization of endogenous human promyelocytic leukemia isoforms. *Cancer Res.* **66**, 6192-6198.
Cuchet, D., Sykes, A., Nicolas, A., Orr, A., Murray, J., Sirma, H., Heeren, J., Bartelt, A. and Everett, R. D. (2011). PML isoforms I and II participate in PML-dependent restriction of HSV-1 replication. *J. Cell Sci.* **124**, 280-291.
de Thé, H., Le Bras, M. and Lallemand-Breitenbach, V. (2012). The cell biology of disease: acute promyelocytic leukemia, arsenic, and PML bodies. *J. Cell Biol.* **198**, 11-21.
di Masi, A., Cilli, D., Berardinelli, F., Talarico, A., Pallavicini, I., Pennisi, R., Leone, S., Antoccia, A., Noguera, N. I., Lo-Coco, F. et al. (2016). PML nuclear body disruption impairs DNA double-strand break sensing and repair in APL. *Cell Death Dis.* **7**, e2308.
El Asmi, F., Maroui, M. A., Dutrieux, J., Blondel, D., Nisole, S. and Chelbi-Alix, M. K. (2014). Implication of PMLIV in both intrinsic and innate immunity. *PLoS Pathog.* **10**, e1003975.
Everett, R. D. and Chelbi-Alix, M. K. (2007). PML and PML nuclear bodies: implications in antiviral defence. *Biochimie* **89**, 819-830.
Fukuda, T., Kigoshi-Tansho, Y., Naganuma, T., Kazaana, A., Okajima, T., Tsuruta, F. and Chiba, T. (2017). CACUL1/CAC1 attenuates p53 activity through PML post-translational modification. *Biochem. Biophys. Res. Commun.* **482**, 863-869.
Geng, Y., Monajembashi, S., Shao, A., Cui, D., He, W., Chen, Z., Hemmerich, P. and Tang, J. (2012). Contribution of the C-terminal regions of promyelocytic leukemia protein (PML) isoforms II and V to PML nuclear body formation. *J. Biol. Chem.* **287**, 30729-30742.
Giorgi, C., Ito, K., Lin, H.-K., Santangelo, C., Wieckowski, M. R., Lebiedzinska, M., Bononi, A., Bonora, M., Duszynski, J., Bernardi, R. et al. (2010). PML regulates apoptosis at endoplasmic reticulum by modulating calcium release. *Science* **330**, 1247-1251.
Guo, L., Giasson, B. I., Glavis-Bloom, A., Brewer, M. D., Shorter, J., Gitler, A. D. and Yang, X. (2014). A cellular system that degrades misfolded proteins and protects against neurodegeneration. *Mol. Cell* **55**, 15-30.
Hands, K. J., Cuchet-Lourenco, D., Everett, R. D. and Hay, R. T. (2014). PML isoforms in response to arsenic: high-resolution analysis of PML body structure and degradation. *J. Cell Sci.* **127**, 365-375.
Hsu, J. K., Lin, T. and Tsai, R. Y. L. (2012). Nucleostemin prevents telomere damage by promoting PML-IV recruitment to SUMOylated TRF1. *J. Cell Biol.* **197**, 613-624.
Ishov, A. M., Sotnikov, A. G., Negorev, D., Vladimirova, O. V., Neff, N., Kamitani, T., Yeh, E. T. H., Strauss, J. F., III and Maul, G. G. (1999). PML is critical for ND10 formation and recruits the PML-interacting protein daxx to this nuclear structure when modified by SUMO-1. *J. Cell Biol.* **147**, 221-234.
Ivanschitz, L., Takahashi, Y., Jollivet, F., Ayrault, O., Le Bras, M. and de Thé, H. (2015). PML IV/ARF interaction enhances p53 SUMO-1 conjugation, activation, and senescence. *Proc. Natl. Acad. Sci. USA* **112**, 14278-14283.
Jensen, K., Shiels, C. and Freemont, P. S. (2001). PML protein isoforms and the RBCC/TRIM motif. *Oncogene* **20**, 7223-7233.
Kamitani, T., Kito, K., Nguyen, H. P., Wada, H., Fukuda-Kamitani, T. and Yeh, E. T. H. (1998). Identification of three major sentrinization sites in PML. *J. Biol. Chem.* **273**, 26675-26682.
Kerscher, O. (2007). SUMO junction - what's your function? New insights through SUMO-interacting motifs. *EMBO Rep.* **8**, 550-555.
Lallemand-Breitenbach, V. and de The, H. (2010). PML nuclear bodies. *Cold Spring Harb. Perspect. Biol.* **2**, a000661.
Lallemand-Breitenbach, V., Zhu, J., Puvion, F., Koken, M., Honore, N., Doubeikovsky, A., Duprez, E., Pandolfi, P. P., Puvion, E., Freemont, P. et al. (2001). Role of promyelocytic leukemia (PML) sumolation in nuclear body formation, 11S proteasome recruitment, and As_2O_3-induced PML or PML/retinoic acid receptor alpha degradation. *J. Exp. Med.* **193**, 1361-1371.
Lang, M., Jegou, T., Chung, I., Richter, K., Munch, S., Udvarhelyi, A., Cremer, C., Hemmerich, P., Engelhardt, J., Hell, S. W. et al. (2010). Three-dimensional organization of promyelocytic leukemia nuclear bodies. *J. Cell Sci.* **123**, 392-400.
Liang, Y.-C., Lee, C.-C., Yao, Y.-L., Lai, C.-C., Schmitz, M. L. and Yang, W.-M. (2016). SUMO5, a novel poly-SUMO isoform, regulates PML nuclear bodies. *Sci. Rep.* **6**, 26509.
Lin, D.-Y., Huang, Y.-S., Jeng, J.-C., Kuo, H.-Y., Chang, C.-C., Chao, T.-T., Ho, C.-C., Chen, Y.-C., Lin, T.-P., Fang, H.-I. et al. (2006). Role of SUMO-interacting motif in Daxx SUMO modification, subnuclear localization, and repression of sumoylated transcription factors. *Mol. Cell* **24**, 341-354.
Maroui, M. A., Pampin, M. and Chelbi-Alix, M. K. (2011). Promyelocytic leukemia isoform IV confers resistance to encephalomyocarditis virus via the sequestration of 3D polymerase in nuclear bodies. *J. Virol.* **85**, 13164-13173.
Maroui, M. A., Kheddache-Atmane, S., El Asmi, F., Dianoux, L., Aubry, M. and Chelbi-Alix, M. K. (2012). Requirement of PML SUMO interacting motif for RNF4- or arsenic trioxide-induced degradation of nuclear PML isoforms. *PLoS ONE* **7**, e44949.
Negorev, D. and Maul, G. G. (2001). Cellular proteins localized at and interacting within ND10/PML nuclear bodies/PODs suggest functions of a nuclear depot. *Oncogene* **20**, 7234-7242.
Nisole, S., Maroui, M. A., Mascle, X. H., Aubry, M. and Chelbi-Alix, M. K. (2013). Differential roles of PML isoforms. *Front. Oncol.* **3**, 125.
Oh, W., Ghim, J., Lee, E.-W., Yang, M.-R., Kim, E. T., Ahn, J.-H. and Song, J. (2009). PML-IV functions as a negative regulator of telomerase by interacting with TERT. *J. Cell Sci.* **122**, 2613-2622.
Ohsaki, Y., Kawai, T., Yoshikawa, Y., Cheng, J., Jokitalo, E. and Fujimoto, T. (2016). PML isoform II plays a critical role in nuclear lipid droplet formation. *J. Cell Biol.* **212**, 29-38.
Pearson, M. and Pelicci, P. G. (2001). PML interaction with p53 and its role in apoptosis and replicative senescence. *Oncogene* **20**, 7250-7256.
Pearson, M., Carbone, R., Sebastiani, C., Cioce, M., Fagioli, M., Saito, S., Higashimoto, Y., Appella, E., Minucci, S., Pandolfi, P. P. et al. (2000). PML regulates p53 acetylation and premature senescence induced by oncogenic Ras. *Nature* **406**, 207-210.
Peche, L. Y., Scolz, M., Ladelfa, M. F., Monte, M. and Schneider, C. (2012). MageA2 restrains cellular senescence by targeting the function of PMLIV/p53 axis at the PML-NBs. *Cell Death Differ.* **19**, 926-936.
Reichelt, M., Wang, L., Sommer, M., Perrino, J., Nour, A. M., Sen, N., Baiker, A., Zerboni, L. and Arvin, A. M. (2011). Entrapment of viral capsids in nuclear PML cages is an intrinsic antiviral host defense against varicella-zoster virus. *PLoS Pathog.* **7**, e1001266.
Sahin, U., de Thé, H. and Lallemand-Breitenbach, V. (2014a). PML nuclear bodies: assembly and oxidative stress-sensitive sumoylation. *Nucleus* **5**, 499-507.
Sahin, U., Ferhi, O., Jeanne, M., Benhenda, S., Berthier, C., Jollivet, F., NIWA-Kawakita, M., Faklaris, O., Setterblad, N., de Thé, H. et al. (2014b). Oxidative stress-induced assembly of PML nuclear bodies controls sumoylation of partner proteins. *J. Cell Biol.* **204**, 931-945.
Salomoni, P. and Pandolfi, P. P. (2002). The role of PML in tumor suppression. *Cell* **108**, 165-170.
Scaglioni, P. P., Yung, T. M., Cai, L. F., Erdjument-Bromage, H., Kaufman, A. J., Singh, B., Teruya-Feldstein, J., Tempst, P. and Pandolfi, P. P. (2006). A CK2-dependent mechanism for degradation of the PML tumor suppressor. *Cell* **126**, 269-283.
Shen, T. H., Lin, H.-K., Scaglioni, P. P., Yung, T. M. and Pandolfi, P. P. (2006). The mechanisms of PML-nuclear body formation. *Mol. Cell* **24**, 331-339.
Shire, K., Wong, A. I., Tatham, M. H., Anderson, O. F., Ripsman, D., Gulstene, S., Moffat, J., Hay, R. T. and Frappier, L. (2016). Identification of RNF168 as a PML nuclear body regulator. *J. Cell Sci.* **129**, 580-591.
Song, J., Durrin, L. K., Wilkinson, T. A., Krontiris, T. G. and Chen, Y. (2004). Identification of a SUMO-binding motif that recognizes SUMO-modified proteins. *Proc. Natl. Acad. Sci. USA* **101**, 14373-14378.
Stehmeier, P. and Muller, S. (2009). Phospho-regulated SUMO interaction modules connect the SUMO system to CK2 signaling. *Mol. Cell* **33**, 400-409.
Sung, K. S., Lee, Y.-A., Kim, E. T., Lee, S.-R., Ahn, J.-H. and Choi, C. Y. (2011). Role of the SUMO-interacting motif in HIPK2 targeting to the PML nuclear bodies and regulation of p53. *Exp. Cell Res.* **317**, 1060-1070.
Tatham, M. H., Geoffroy, M.-C., Shen, L., Plechanovova, A., Hattersley, N., Jaffray, E. G., Palvimo, J. J. and Hay, R. T. (2008). RNF4 is a poly-SUMO-specific E3 ubiquitin ligase required for arsenic-induced PML degradation. *Nat. Cell Biol.* **10**, 538-546.
Weidtkamp-Peters, S., Lenser, T., Negorev, D., Gerstner, N., Hofmann, T. G., Schwanitz, G., Hoischen, C., Maul, G., Dittrich, P. and Hemmerich, P. (2008).

Journal of Cell Science (2017) 130, 3496-3506 doi:10.1242/jcs.202879

Dynamics of component exchange at PML nuclear bodies. *J. Cell Sci.* **121**, 2731-2743.

Zhang, J., Shi, D., Li, X., Ding, L., Tang, J., Liu, C., Shirahige, K., Cao, Q. and Lou, H. (2017). Rtt101-Mms1-Mms22 coordinates replication-coupled sister chromatid cohesion and nucleosome assembly. *EMBO Rep.* **18**, 1294-1305.

Zhong, S., Muller, S., Ronchetti, S., Freemont, P. S., Dejean, A. and Pandolfi, P. P. (2000a). Role of SUMO-1-modified PML in nuclear body formation. *Blood* **95**, 2748-2752.

Zhong, S., Salomoni, P. and Pandolfi, P. P. (2000b). The transcriptional role of PML and the nuclear body. *Nat. Cell Biol.* **2**, E85-E90.